Alma Mater Studiorum · Università di Bologna

SCUOLA DI SCIENZE

Corso di Laurea Magistrale in Matematica

COMPRESSED SENSING IN DIGITAL TOMOSYNTHESIS RECONSTRUCTION

Tesi di Laurea in Analisi Numerica

Relatore:
Chiar.ma Prof.ssa
Elena Loli Piccolomini

Presentata da:
Alessia Magnani

II Sessione
Anno Accademico 2014-2015

If people do not believe that mathematics is simple,
it is only because they do not realize how complicated life is.
John von Neumann

Introduction

Digital Tomosynthesis (DT) is an X-ray based tomographic imaging technique. It is a non-invasive and non-destructive method for the three-dimensional visualization of the inner structures of an object, in which the projection-view images are acquired at a limited number of angles over a limited angular range.

DT is known as an attractive low-dose alternative to Computed Tomography (CT) in medical and non-medical imaging applications, when the data acquisition over the full angular range is impossible or infeasible if the object is too large or if only a small part of the object is of interest.

The primary application of DT is the screening of breast cancer, DT is used together with traditional mammography for the detection of microcalcifications and tumors.

The problem of reconstructing 3D images from the projections provided in the Digital Tomosynthesis is an ill-posed inverse problem.

The standard strategy to solve this kind of problem is to minimize an object function that contains a data fitting term and a regularization term.

The data fitting term is generally represented by the square of the 2-norm of the residual, namely we generally search for the solution of a least squares problem, and the regularization term is a function of the norm of the solution.

The contribution of this thesis is to use the techniques of the compressed sensing, in particular replacing the least squares problem of data fitting with the problem of minimizing the 1-norm of the residuals, and using as regularization term the Total Variation (TV).

We will propose two different algorithms: a new alternating minimization algorithm, and a version of the more standard scaled projected gradient algorithm that involves the 1-norm.

The first chapter contains some general notions on digital tomosynthesis, on the mathematical model of image reconstruction, and the tools involved in the resolution of this problem. In particular it describes the system matrix, the functional object of the minimization problem that involves the 1-norm of the residual, and some recalls on the total variation.

In the second chapter we described a minimizing alternating method, with its convergence results, and we show the numerical results obtained from testing the algorithm on noisy projections of the CIRS phantom.

In the third chapter an algorithm of scaled and projected gradient is presented in which we have replaced the data fitting term with the 1-norm of the residual, and we show the convergence results for this method and the experiments of the algorithm on the same CIRS phantom of Chapter 2.

Introduzione

La tomosintesi digitale (DT) è una tecnica di imaging tomografica basata sui raggi X. È un metodo non invasivo e non distruttivo per la visualizzazione tridimensionale delle strutture interne di un oggetto, nel quale le proiezioni sono acquisite ad un numero limitato di angoli in un limitato range angolare. La DT è nota come una conveniente alternativa alla tomosintesi computerizzata (CT) a bassa dose di radiazioni, utilizzata nelle applicazioni mediche e non mediche, utile quando l'acquisizione dei dati a 360 gradi è impossibile o non attuabile, se l'oggetto è troppo grande o se si interessati a indagare solo una parte di esso.

L'applicazione primaria della DT è lo screening del cancro al seno, per individuare insieme alla mammografia tradizionale le microcalcificazioni e i tumori.

Il problema di ricostruire immagini 3D a partire dalle proiezioni fornite della tomosintesi digitale è un problema inverso mal posto.

La strategia standard per risolvere questo genere di problema è quello di minimizzare una funzione oggetto che contiene una parte di fitting dei dati e una parte di regolarizzazione. Il fitting dei dati è generalmente rappresentato dal quadrato della norma 2 del residuo, ovvero si cerca la soluzione di un problema di minimi quadrati, e il termine di regolarizzazione è una funzione della norma della soluzione.

Il contributo di questa tesi è quello di utilizzare le tecniche del *compressed sensing* in particolare sostituendo il problema di minimi quadrati nel fitting dei dati con il problema di minimizzare la norma 1 del residuo e utilizzando come termine di regolarizzazione la variazione totale (TV).

Proporremo due diversi algoritmi: un nuovo algoritmo di minimizzazione alternata, e una versione del più standard algoritmo del gradiente scalato e proiettato che coinvolge la norma 1.

Nel primo capitolo sono richiamate alcune nozioni generali sia sulla tomosintesi digitale che sul modello e sugli strumenti matematici coinvolti nella risoluzione del problema. In particolare è descritta la matrice del sistema, il funzionale oggetto del problema di minimo che coinvolge la norma 1 del residuo, e alcuni richiami sulla variazione totale.

Nel secondo capitolo è descritto il metodo di minimizzazione alternata, con i risultati di convergenza di tale metodo, e sono riportati i risultati numerici ottenuti dalla sperimentazione dell'algoritmo su proiezioni rumorose del fantoccio CIRS con livello di rumore pari a 10^{-3}

Nel terzo capitolo è infine presentato un algoritmo di gradiente scalato e proiettato in cui abbiamo sostituito la parte di fitting dei dati con la norma 1 del residuo, e anche per questo metodo sono riportati i risultati di convergenza e le sperimentazioni dell'algoritmo sul medesimo fantoccio CIRS del Capitolo 2.

Contents

Introduction **i**

Introduction **iii**

1 Digital tomosynthesis model and Total Variation **1**

1.1 Digital tomosynthesis 1

1.2 Mathematical model 2

1.3 Total Variation 6

1.3.1 Numerical methods for Total Variation 7

1.3.2 A one-dimensional discretization 7

1.3.3 A three-dimensional discretization 8

2 An Alternating Minimization Algorithm **11**

2.1 Introduction to the algorithm 11

2.1.1 Notation 12

2.1.2 An alterating minimization algorithm 13

2.2 Convergence analysis 16

2.3 Numerical results 20

2.3.1 Test problem 20

2.3.2 Numerical experiments 22

3 Scaled Projected Gradient Method **33**

3.1 Definition and basic properties 33

3.2 The SGP method 34

3.3 Convergence analysis 36

3.4 The SGP method for 3D image reconstruction 39

3.4.1 Update the scaling matrix 40

3.4.2 Update the steplength 40

3.5 Numerical results 42

List of Figures

2.1 Cirs phantom 21
2.2 ADM reconstruction 23
2.3 ADM relative error 24
2.4 Recostruction comparison (central layer) 24
2.5 Recostruction comparison (layer 9) 25
2.6 Comparison of the different structures recostructions (central layer) 26
2.7 Comparison of the different structures recostructions (layer 9) 27
2.8 Recostructions after 10, 30 and 60 seconds (layer 8) 28
2.9 Comparison of the different structures recostructions after 30 seconds (central layer) 29
2.10 SNR in each layer 31

3.1 SGP reconstruction 44
3.2 SGP relative error 45
3.3 Recostruction comparison (central layer) 45
3.4 Recostruction comparison (layer 9) 46
3.5 Comparison of the different structures recostructions (central layer) 47
3.6 Comparison of the different structures recostructions (layer 9) 48

3.7 Recostructions after 10, 30 and 60 seconds (layer 8) 49
3.8 Comparison of the different structures recostructions after 30 seconds (central layer) 50
3.9 SNR in each layer 51

Chapter 1

Digital tomosynthesis model and Total Variation

1.1 Digital tomosynthesis

Digital tomosynthesis (DT) is an X-ray based limited angle imaging technique. In tomosynthesis projection images are acquired over a limited angular range. It is a non-invasive and non-destructive method for three-dimensional visualization of the inner structures of an object. Computed radiography (CR) and digital radiography (DR) are used for planar imaging when a three-dimensional object is mapped onto a two-dimensional plane. Tomosynthesis is historically the first X-ray based tomographic technique. However, it has been forgotten with the development of computed tomography (CT). Only recently, developments in the field of digital X-ray detectors and computer technologies have led to a renewed interest in this technique. A high in-plane resolution, three-dimensionality and a low radiation dose make DT an attractive alternative to CT in many imaging applications. The most widely used DT application in medical imaging is breast imaging, DT is used together

with traditional mammography for the detection of microcalcifications and masses. In contrast to CT, the DT projection dataset is incomplete, because the X-ray source and the detector do not completely rotate around the patient. Although DT is a volumetric imaging technique and provides dimensional information about the location of structures, the complete three-dimensional information about the object cannot be reconstructed. Therefore, one of the major issues is the improvement of the tomosynthesis image quality.

1.2 Mathematical model

A DT data acquisition includes measuring a limited number of low-dose two-dimensional projections of an object. This is done by moving a detector and an X-ray tube around the object within a limited angular range.
The restricted quantity of data measured by DT leads to the compressed sensing (CS): in data processing, the traditional practice is to measure (sense) data in full length and then compress the resulting measurements before storage or transmission. In such a scheme, recovery of data is generally straightforward. This traditional data-acquisition process can be described as "full sensing plus compressing".
Compressed sensing, also known as compressive sensing or compressive sampling, represents a paradigm shift in which the number of measurements is reduced during acquisition so that no additional compression is necessary. The price to pay is that more sophisticated recovery procedures become necessary.
In particular in DT each measured two-dimensional intensity image $I(f;\theta)$ represents the decreased signal, where f is measured object. The decrease

is caused by photon-matter interactions. If no object is present, the initial intensity I_0 will be measured. The model of tomosynthesis measurements is based on the well known exponential Beer-Lambert law for a monoenergetic spectrum

$$I(f;\theta) = I_0 e^{-\int_L \mu(x)\,dx} \tag{1.1}$$

A projection image $g(f;\theta)$ has a linear relation to the attenuation coefficients $\mu(x)$ and is defined as

$$g(f;\theta) = \int_L \mu(x)\,dx \tag{1.2}$$

So we can write the image reconstruction problem as

$$g = Kf \tag{1.3}$$

where f is the exaxt image, and K is the model of emission and detection process described above.

Image reconstruction consists in solving equation (1.3) in order to determine the value of f, based on a set of observation of g. This problem can not be linearly solved due too the high number of f values to be calculated, and to the high number of g values to be considered. One of the ways of finding the solution of the problem will pass by an iterative process of gradually approaching an estimation of f to its real values. The success of this task will be highly dependent on the iterative procedure used to approach the estimation to the real values and from how realistic is the model K in (1.3). Since we have a finite number of measurements, we have to consider the observation g in a discrete form g_i, having a value for each possible Line of Response (LOR) i. We can also assume that the image f can be approximated by a linear combination of a finite set of basis functions f_i, which are known as voxels, namely cube-shaped elements covering the 3D space. When looking to the problem from this perspective, we should rewrite (1.3)

into (1.4)

$$g_i = \sum_j K_{i,j} f_j \tag{1.4}$$

In this new formulation, the process of emission and detection can now be seen as a matrix, composed of elements $K_{i,j}$.

In this thesis the system matrix K is calculated by a ray-driven method described in [5], in which each system matrix element is defined as the length of segment of the LOR i in the voxel j.

It is important to note that although the line integrals g are measured, the image f is of interest

$$f = K^{-1} g$$

However, the direct matrix inversion of this equation is practically infeasible due to the large size of the equation system. Moreover, in the case of limited angle tomosynthesis acquisition geometry, this system is severely under-determined.

This leads to the need of an alternative algorithm. One such approach is to formulate an optimization problem, which minimizes some pre-defined cost function to find the

$$f = arg \min_{f \geq 0} T(f)$$

The cost function is constructed of two components: a data fitting term and a regularization or penalty term with a regularization parameter μ

$$T(f) = DataFitting(g; Kf) + \mu RegularizationTerm(f)$$

In this thesis we chose as data fitting term

$$\|Kf - g\|_1$$

instead of the more classical least squares term

$$\|Kf - g\|_2^2$$

in order to increase the sparsity of the solution.
There are two main classes of regularizer:

- The first one is the Tikhonov-like category, including $RegularizationTerm(f) = \sum_j \|D_j f\|^2$ where D_j's stands for a finite difference operator; in these methods the resulting objective functions $T(f)$ are quadratic so is relative simple to minimize them. However Tikhonov-like regularizers tend to produce a solution overly smooth, and rarely succeed to maintain important image details such as sharp edges.

- The second class of regularizer employs the Total Variation (TV).
  The methods of this class can better preserve sharp edges or object boundaries that are usually the most important features to recover, however the TV model is computionally more difficult to solve.

For these reasons we chose as penalty term the Total Variation and we obtained a method designed to give piece-wise constant solutions.
We want to solve the minimization problem

$$minT(f) = \|Kf - g\|_1 + \mu TV(f) \tag{1.5}$$

In the next section we briefly discuss some of the Total Variation properties and its discretized form.

1.3 Total Variation

We begin our discussion over Total Variation with the classical definition of Total Variation of a function f defined on the interval $[0, 1]$

$$TV(f) = \sup \sum_i |f(x_i) - f(x_{i-1})| \tag{1.6}$$

where supremum is taken over all partition $0 = x_0 < x_1 < \cdots < x_n = 1$ of interval. If f is piecewise constant with a finite number of jump discontinuities, then $TV(f)$ gives the sum of the magnitudes of the jump, if f is smooth, one can multiply and divide the right hand side of (1.6) by $\Delta x_i = x_i - x_{i-1}$ and take the limits as the $\Delta x_i \to 0$ to obtain the representation

$$TV(f) = \int_0^1 |\frac{df}{dx}| \, dx \tag{1.7}$$

An obvious generalization of (1.7) to three-dimensional space dimension is

$$TV(f) = \int_0^1 \int_0^1 \int_0^1 |\nabla f| \, dx \, dy \, dz \tag{1.8}$$

where $\nabla f = (\frac{\partial f}{\partial x}, \frac{\partial f}{\partial y}, \frac{\partial f}{\partial z})$ denotes the gradient, and $|(x, y, z)| = \sqrt{x^2 + y^2 + z^2}$ denotes the Euclidian norm.

$TV(f)$ can be interpretated geometrically as the lateral surface area of the graph of f, if f has many large amplitude oscillation, then it has large lateral surface area, and hence $TV(f)$ is large.

Then it is easy to understand why Total Variation is useful in image reconstruction: with Total Variation one can effectively reconstruct function with jumps discontinuity, and this reconstruction tends to produce qualitatively correct reconstructions of blocky images.

By blocky we mean that the image is nearly piecewise constant with discontinities, and the length of the curves on which the discontinuities occur is relatively small.

1.3.1 Numerical methods for Total Variation

We want to obtain regularization solution to operator equation described in (1.3) by minimizing the functional

$$T(f) = \|Kf - g\|_1 + \mu TV(f) \tag{1.9}$$

However, the representation (1.7) is not suitable for the implementation of the numerical methods that we will present in Chapter 2 and Chapter 3 due to the non-differentiability of the Euclidean norm at the origin. To overcome this difficulty, one can take an approximation of the Euclidean norm $|(x, y, z)|$ like this $\sqrt{x^2 + y^2 + z^2 + \beta^2}$ where β is a small positive parameter.
This yelds the following approximation of $TV(f)$, valid for a smooth function f defined on the unit interval in one dimension

$$J_\beta(f) = \int_0^1 \sqrt{\left(\frac{df}{dx}\right)^2 + \beta^2}\, dx$$

In three space dimensions, this becomes

$$J_\beta(f) = \int_0^1 \int_0^1 \int_0^1 \sqrt{\left(\frac{df}{dx}\right)^2 + \left(\frac{df}{dy}\right)^2 + \left(\frac{df}{dz}\right)^2 + \beta^2}\, dx\, dy\, dz \tag{1.10}$$

1.3.2 A one-dimensional discretization

Now we need to represent the approximation of Total Variation given above in a discete form. We first present a one-dimensional discretization that will be generalized for the three-dimensional space case.
Let us suppose $f(x)$ is a smooth function defined on the unit interval in $\mathbb{R}$ and $\mathbf{f} = (f_0, \ldots, f_n)$ with $f_i \approx f(x_i), x_i = i\Delta x, \Delta x = 1/n$. Take the derivative approximation

$$D_i\mathbf{f} = \frac{f_i - f_{i-1}}{\Delta x}, \quad i = 1, \ldots, n$$

with the matrix representation $D_i = [0, \ldots, 0, -1/\Delta x, 1/\Delta x, 0, \ldots, 0]$.

We assume a discretized penalty functional of the form

$$J(f) = \frac{1}{2} \sum_{i=1}^{n} \psi\left((D_i \mathbf{f})^2\right) \Delta x \tag{1.11}$$

where ψ is a smooth approximation to twice the square root function $\psi(t) = 2\sqrt{t + \beta^2}$

To minimize (1.9) we need the gradient of J. For any $\mathbf{v} \in \mathbb{R}^{n+1}$,

$$\frac{d}{d\tau} J(\mathbf{f} + \tau \mathbf{v}) = \sum_{i=1}^{n} \psi'\left((D_i \mathbf{f})^2\right) (D_i \mathbf{f})(D_i \mathbf{v}) \Delta x \tag{1.12}$$

$$= \Delta x (D\mathbf{v})^T \mathrm{diag}(\psi'(\mathbf{f}))(D\mathbf{f}) \tag{1.13}$$

$$= \langle \Delta x (D\mathbf{v})^T \mathrm{diag}(\psi'(\mathbf{f}))(D\mathbf{f}), \mathbf{v} \rangle \tag{1.14}$$

where $\mathrm{diag}(\psi'(\mathbf{f}))$ denotes the $n \times n$ diagonal matrix whose ith diagonal entry is $(\psi'((D_i \mathbf{f})^2)$, D is the $n \times (n+1)$ matrix whose ith row is D_i, and $\langle \cdot, \cdot \rangle$ denotes the Euclidean inner product on $\mathbb{R}^{n+1}$.

From this we obtain the gradient

$$\mathrm{grad} J(\mathbf{f}) = L(\mathbf{f})\mathbf{f} \tag{1.15}$$

$$L(\mathbf{f}) = \Delta x D^T \mathrm{diag}(\psi'(\mathbf{f}))D \tag{1.16}$$

where $L(\mathbf{f})$ is a symmetric positive semidefinite $(n+1) \times (n+1)$ matrix.

1.3.3 A three-dimensional discretization

We now generalized the discretization given above at the three-dimensional case.

Suppose $f = f_{ijk}$ is defined on an equispaced grid in three space dimensions, $\{(x_i, y_j, z_k) | x_i = i\Delta x, y_j = l\Delta y, z_k = k\Delta z, i = 0, \ldots, n_x, j = 0, \ldots, n_y,$

$k = 0, \ldots, n_z\}$. In an analogous manner to the one-dimensional case, we define the discrete penalty functional

$$J(f) = \frac{1}{2} \sum_{i=1}^{n_x} \sum_{j=1}^{n_y} \sum_{k=1}^{n_z} \psi \left((D^x_{ijk} f)^2 + (D^y_{ijk} f)^2 + (D^z_{ijk} f)^2 \right) \tag{1.17}$$

where

$$D^x_{ijk} f = \frac{f_{i,j,k} - f_{i-1,j,k}}{\Delta x}, \quad D^y_{ijk} f = \frac{f_{i,j,k} - f_{i,j-1,k}}{\Delta y}, \quad D^z_{ijk} f = \frac{f_{i,j,k} - f_{i,j,k-1}}{\Delta z} \tag{1.18}$$

To simplify the notation we dropped the factor $\Delta x \Delta y \Delta z$ from the right-hand side of (1.17); this factor can be absorbed in the regularization paramenter μ in (1.9).

Gradient computations are similar to those in one dimension

$$\frac{d}{d\tau} J(f+\tau v)|_{\tau=0} = \sum_{i=1}^{n_x} \sum_{j=1}^{n_y} \sum_{k=1}^{n_z} \psi'_{ijk} \left[(D^x_{ijk} f)(D^x_{ijk} v) + (D^y_{ijk} f)(D^y_{ijk} v) + (D^z_{ijk} f)(D^z_{ijk} v) \right]$$

where $\psi'_{ijk} = \psi'((D^x_{ijk} f)^2 + (D^y_{ijk} f)^2 + (D^z_{ijk} f)^2))$.

Now let $\mathbf{f} = \mathbf{vec}(f)$ and $\mathbf{v} = \mathbf{vec}(v)$, corresponding to lexicographical column ordering of the three-dimensional array components, let D_x, D_y and D_z denote the resulting $n_x n_y n_z \times (n_x + 1)(n_y + 1)(n_z + 1)$ matrices corresponding to the grid operator in (1.18), let $\mathrm{diag}(\psi'(\mathbf{f}))$ denote the $n_x n_y n_z \times n_x n_y n_z$ diagonal matrix whose diagonal entries are the ψ'_{ijk}s and let $\langle \cdot, \cdot \rangle$ denotes the Euclidean inner product on $\mathbb{R}^{(n_x+1)(n_y+1)(n_z+1)}$. Then

$$\begin{aligned} \frac{d}{d\tau} J(f + \tau v)|_{\tau=0} =& \langle \mathrm{diag}(\psi'(\mathbf{f}))(D_x \mathbf{f}), D_x \mathbf{v} \rangle + \langle \mathrm{diag}(\psi'(\mathbf{f}))(D_y \mathbf{f}), D_y \mathbf{v} \rangle + \\ &+ \langle \mathrm{diag}(\psi'(\mathbf{f}))(D_z \mathbf{f}), D_z \mathbf{v} \rangle \end{aligned}$$

From this we obtain a gradient representation like (1.15), but now

$$L(\mathbf{f}) = D_x^T \mathrm{diag}(\psi'(\mathbf{f}))D_x + D_y^T \mathrm{diag}(\psi'(\mathbf{f}))D_y + D_z^T \mathrm{diag}(\psi'(\mathbf{f}))D_z = \quad (1.19)$$

$$= [D_x^T D_y^T D_z^T] \begin{bmatrix} \mathrm{diag}(\psi'(\mathbf{f})) & 0 & 0 \\ 0 & \mathrm{diag}(\psi'(\mathbf{f})) & 0 \\ 0 & 0 & \mathrm{diag}(\psi'(\mathbf{f})) \end{bmatrix} \begin{bmatrix} D_x \\ D_y \\ D_z \end{bmatrix} \quad (1.20)$$

We now have a discrete representation of the minimization problem described in (1.5), and we can present the numerical methods to find its solution.

Chapter 2

An Alternating Minimization Algorithm

2.1 Introduction to the algorithm

In this chapter we introduce an algorithm for recostructing 3D data from noisy projections.

The algorithm we are going to describe is a modified version of the alternating minimization method for Total Variation image recostruction proposed in [3] and in [4] by Wang Y., Yang J. and Zhang Y., that we readjusted to recostruct 3D data.

Let $f \in \mathbb{R}^{n^2 m}$ be an original $n \times n \times m$ grayscale object, K represent a blurring operator, ω be additive noise, and g be an observation that satisfies the relationship

$$g = Kf + \omega \tag{2.1}$$

Then, give K and g, f is recoverd from the model

(2.2)

where $D_i f \in \mathbb{R}^3$ denotes the discete gradient of f, and the sum $\sum \|D_i f\|$ is the discrete Total Variation of f.

Since TV norms are essentially L_1 norms of derivatives, L_1 estimation procedures are more appropriate for the subject of image restoration.

Our algorithm used a variable-splitting and penalty techniques in optimization, specifically let $z \in \mathbb{R}^{n^2 m}$ be an auxiliary variable that approximates $Kf - g$ and for each voxel let $\mathbf{w}_i \in \mathbb{R}^3$ an auxiliary variable introduced to transfer $D_i f$ out of the nondifferential term $\|\cdot\|_1$. For convenience, we let $\mathbf{w} = [\mathbf{w}_1, \dots \mathbf{w}_{n^2 m}]$.

Then, by adding quadratic terms to penalize the difference between every pair of original an auxiliary variables, we obtain the following approximation problem

$$\min_{\mathbf{w},z,f} \sum_i \left(\|\mathbf{w}_i\|_1 + \frac{\beta_1}{2} \|\mathbf{w}_i - D_i f\|_1^2 \right) + \mu \|z\|_1 + \frac{\beta_2}{2} \|z - (Kf - g)\|_1^2 \quad (2.3)$$

with a sufficiently large parameters β_1 and β_2.

From the theory of penalty methods, the solutions of (2.3) converge to that of (2.2) as the penalty parameters go to infinity.

The motivation for this formulation is that it is numerically easier to minimize by an iterative and alternating approach, due to the fact that with any two of the three variables $\mathbf{w}, z$, and f fixed, the minimizer of (2.3) with respect to the third one has a closed-form formula that is easy to compute.

In addiction this approach is numerical stable for large values of β_1 and β_2.

2.1.1 Notation

Let $D^{(j)} \in \mathbb{R}^{n^2 m \times n^2 m}$ be finite differences matrices, and in particular let $D^{(1)}, D^{(2)}$ and $D^{(3)}$ be the first-order forward finite difference matrices with appropriate boundary conditions in the three different directions respectively.

As is used in (2.2), $D_i \in \mathbb{R}^{3n^2m}$ is a three-row matrix formed by stacking the ith rows of $D^{(1)}, D^{(2)}$ and $D^{(3)}$.

From here the norm $\|\cdot\|$ refers to the 1-norm.

We introduce three auxiliary vectors w_1, w_2 and w_3 to approximate $D^{(1)}f, D^{(2)}f$ and $D^{(3)}f$ respectively; we denote $w = (w_1, w_2, w_3) \in \mathbb{R}^{3n^2m}$ and $D = (D^{(1)}, D^{(2)}, D^{(3)}) \in \mathbb{R}^{3n^2m \times n^2m}$.

2.1.2 An alterating minimization algorithm

We begin with assuming $\beta_1 = \beta_2 \equiv \beta$ in (2.3) which does not cause loss of generality.

It is easy to see that for a fixed f the minimization with respect to $\mathbf{w}$ and z can be done in parallel because they are separable in (2.3). In addition, for all subscript i, the first two term in (2.3) are separable with respect to $\mathbf{w}_i$ and the last two terms are separable with respect to each component of z.

Based on these observations, it is easy to apply alternating minimization to (2.3): first for a fixed f the minimizer function of $\mathbf{w}_i$ is given by a multidimensional shrinkage

$$\mathbf{w}_i = max\left\{\|D_i f\| - \frac{1}{\beta}, 0\right\} \operatorname{sgn}(D_i f)\ ,\ i = 1, 2, \cdots, n^2m \tag{2.4}$$

where the convenction $0 \cdot (\frac{0}{0}) = 0$ is followed. The minimization with respect to z is given by the one-dimensional shrinkage:

$$z = max\left\{|Kf - g| - \frac{\mu}{\beta}, 0\right\} \circ \operatorname{sgn}(Kf - g) \tag{2.5}$$

where $\circ$ represents the pointwise product, and all other operations are implemented componentwise.

Second, for fixed $\mathbf{w}$ and z, the minimization with respect to f is a least

squares problem:

$$min_f \sum_i \|\mathbf{w}_i - D_i f\|_1^2 + \|Kf - (g+z)\|_1^2 \tag{2.6}$$

In this thesis we solve the least squares problem using the conjugate gradient method for least squares problem (CGLS) with a relative stopping condition on the residual norm in addition to a condition on the maximum number of iterations.

Is well known that the CGLS method solves a lineare least squares problem

$$\min_x \Phi(x) = \frac{1}{2}\|Qx - c\|^2 = \frac{1}{2}x^T Q^T Q x - x^T Q^T c \tag{2.7}$$

that is a quadratic form problem where $Q \in \mathbb{R}^{m\times n}$, $n \leq m$. Solve (2.7) is equivalent to solve the normal equations system

$$Q^T Q x = Q^T c \tag{2.8}$$

If the matrix $Q^T Q$ is positive definite we can use the CG method in order to solve (2.8).

Now we present the pseudo-code of the CGLS algorithm:

Algorithm 1: CG method for least squares problem

Given $x_0 \in \mathbb{R}^n$, $tol > 0$

$r_0 \leftarrow b - Qx_0$, $z_0 \leftarrow Q^T r_0$, $p_0 = z_0$, $k \leftarrow 0$;

while $norm(r_k) \geq tol$ **do**

$w_k \leftarrow Qp_k$;

$\alpha_k \leftarrow \frac{z_k^T z_k}{w_k^T w_k}$;

$x_{k+1} \leftarrow x_k + \alpha_k p_k$;

$r_{k+1} \leftarrow r_k - \alpha_k w_k$;

$z_{k+1} \leftarrow Q^T r_{k+1}$;

$\beta_{k+1} \leftarrow \frac{z_{k+1}^T z_{k+1}}{z_k^T z_k}$;

$p_{k+1} \leftarrow z_{k+1} + \beta_{k+1} p_k$;

$k \leftarrow k + 1$;

end

We present the scheme for the alternating minimization algorithm we described:

Algorithm 2: ADM methods with CG

Given $g, K, \mu > 0$, *and* $\beta > 0$.

$f \leftarrow g$;

while *"not converged"* **do**

(1) Given f, *compute* $\mathbf{w}$ *and* z *by (2.4) and (2.5) respectively*;

(2) Given $\mathbf{w}$ *and* z *compute* f *by solving (2.6) using CGLS* ;

end

There is two stopping conditions for the extern cycle, one is the maximum number of iteration criteria, that stops the algorithm at the 2000th iteration, the other is a condition based on semiconvergence: we stopped it when the

relative error of the current iteration overcomes the error at the previous one.

2.2 Convergence analysis

In this section we analyse the convergence property of Algorithm 2 for a fixed $\beta > 0$; we will omit most of the proofs, but the reader can refer to [3].
First we prove that the sequence $\{(w^k, f^k)\}$ generated by Algorithm 2 from any initial point converges to a solution of (2.3).
For $t \in \mathbb{R}$, let the one-dimensional shrinkage de defined by

$$s_\mu(t) = max\left\{|t| - \tfrac{\mu}{\beta}, 0\right\} \cdot \text{sgn}(t)$$

For $\mathbf{t} \in \mathbb{R}^3$ we define the three-dimensional shrinkage operator $s : \mathbb{R}^3 \to \mathbb{R}^3$ as

$$s(\mathbf{t}) = max\left\{\|\mathbf{t}\| - \tfrac{1}{\beta}, 0\right\} \frac{\mathbf{t}}{\|\mathbf{t}\|}$$

where the convention $0 \cdot (0/0) = 0$ is followed.
It is easy to see that

$$s(a) = a - \mathcal{P}(a)$$

where $\mathcal{P} : \mathbb{R}^3 \to \mathbb{R}^3$ is the projection onto the closed ball $\mathcal{B} = \{\mathbf{t} \in \mathbb{R}^3, \|\mathbf{t}\| \leq \frac{1}{\beta}\}$ For $v \in \mathcal{R}^N$, let $s_\mu(v) = (s_\mu(v_1); \ldots; s_\mu(v_N)) \in \mathbb{R}^N$.
For vectors $f, v, w \in \mathcal{R}^N$, $N \geq 1$ is defined $S(f, v, w) : \mathbb{R}^{3N} \to \mathbb{R}^{3N}$ as

$$S(f, v, w) = (s(\mathbf{t}_1); \ldots; s(\mathbf{t}_N)) \text{ where } \mathbf{t}_i = \begin{bmatrix} f_i \\ v_i \\ w_i \end{bmatrix}$$

namely S applies three-dimensional shrinkage to each triplet $(f_i, v_i, w_i) \in \mathbb{R}^3$ for $i = 1, \ldots N$.

The first convergence result is (2.2.1) and we take a few step to prove it: first we prove the nonexpansiveness of the shrinkage operator s.

Proposition 2.2.1. *For any* $\mathbf{t}_1, \mathbf{t}_2 \in \mathbb{R}^3$*, it holds that*

$$\|s(\mathbf{t}_1) - s(\mathbf{t}_2)\|^2 \leq \|\mathbf{t}_1 - \mathbf{t}_2\|^2 - \|\mathcal{P}(\mathbf{t}_1) - \mathcal{P}(\mathbf{t}_2)\|^2$$

Furthermore, if $\|s(\mathbf{t}_1) - s(\mathbf{t}_2)\| = \|\mathbf{t}_1 - \mathbf{t}_2\|$*, then* $s(\mathbf{t}_1) - s(\mathbf{t}_2) = \mathbf{t}_1 - \mathbf{t}_2$.

We will make use of a mild assumption in our convergence analysis:
Assumption 1 $\mathcal{N}(K) \cap \mathcal{N}(D) = \{0\}$, where $\mathcal{N}(\cdot)$ represents the null space of a matrix.
We will use the following two symmetric and positive definite matrix:

$$H = (D; K) \text{ and } M = D^T D + K^T K = H^T H \tag{2.9}$$

and Assumption 1 ensures that M^{-1} is well defined. Furthermore let $v = (w; z)$ we also define the operator $\hat{h} : \mathbb{R}^{3n^3} \to \mathbb{R}^{3n^3}$ as $\hat{h}(v) = (h(v); h^{(3)}(v))$ where $h(v) = (h^{(1)}(v), h^{(2)}(v))$, and

$$h^{(j)}(v) = D^{(j)} M^{-1} \left(H^T v + K^T g \right), \, j = 1, 2$$

$$h^{(3)}(v) = K M^{-1} (H^T v + K^T g) - g$$

Let $\hat{S} \circ \hat{h} = (S \circ h; s_\mu \circ h^{(3)})$ Using the above notation we can rewrite the two iterative steps of Algorithm 2 as

$$v^{k+1} = (w^{k+1}, z^{k+1}) = S(D^{(1)} f^k; D^{(2)} f^k; D^{(3)} f^k; s_\mu(K f^k - g)) = \hat{S} \circ \hat{h}(v^k), \tag{2.10}$$

$$f^{k+1} = M^{-1} \left(H^T v^{k+1} + K^T g \right) \tag{2.11}$$

Since the objective function in (2.3) is convex, bounded below, and coercive (its value goes to infinity as $\|(w, z, f)\| \to \infty$)), (2.3) has at least one minimizer pair $(v^*, f^*) = (w^*, z^*, f^*)$ that must satisfy

$$v^* = S(D^{(1)} f^*; D^{(2)} f^*; D^{(3)} f^*; s_\mu(K f^* - g)) = \hat{S} \circ \hat{h}(v^*), \tag{2.12}$$

$$f^* = M^{-1}\left(H^T v^* + K^T g\right) \tag{2.13}$$

In particular (2.12) means that v^* is a fixed point of $\hat{S} \circ \hat{h}$.
Now we show that $\hat{h}$ is nonexpansive

Proposition 2.2.2. *For any $v_1 \neq v_2 \in \mathbb{R}^{3n^3}$, it holds that*

$$\|\hat{h}(v_1) - \hat{h}(v_2)\| \leq \|v_1 - v_2\|$$

and the equality holds if and only if $\hat{h}(v_1) - \hat{h}(v_2) = v_1 - v_2$.

Then the following lemma gives a useful property for fixed points of the operator $\hat{S} \circ \hat{h}$:

Lemma 2.2.1. *Let v^* be any fixed point of $\hat{S} \circ \hat{h}$. For any v we have $\|\hat{S} \circ \hat{h}(v^*)\| < \|v - v^*\|$ unless v is a fixed point of $\hat{S} \circ \hat{h}$.*

Now we are ready to prove the convergence of Algorithm 2.

Theorem 2.2.1. *For any fixed $\beta > 0$ under Assumption 1 the sequence $\{(w^k, z^k, f^k)\}$ generated by Algorithm 2 from any starting point (w^0, z^0, f^0) converges to a solution (w^*, z^*, f^*) di (2.3).*

Proof. From non expansiveness of $\hat{S} \circ \hat{h}$ it is easy to show that the sequence v^k lies in a compact region, and thus it have at least one limit point $v^* = \lim_{j\to\infty} v^{k_j}$.
Letting $\hat{v}$ be any fixed point of $\hat{S} \circ \hat{h}$, namely $\hat{S} \circ \hat{h}(\hat{v}) = \hat{v}$, we get

$$||v^k - \hat{v}|| = ||\hat{S} \circ \hat{h}(v^{k-1}) - \hat{S} \circ \hat{h}(\hat{v})|| \leq ||v^{k-1} - \hat{v}||$$

from the lemma 2.2.1, and so the following limit exists

$$\lim_{k\to\infty} ||v^k - \hat{v}|| = \lim_{j\to\infty} ||v^{k_j} - \hat{v}|| = ||v^* - \hat{v}|| \tag{2.14}$$

Namely all limit points of the sequence v^k, if more than one, have all equal distance from $\hat{v}$.

By the continuity of $\hat{S} \circ \hat{h}$ we can state that

$$\hat{S} \circ \hat{h}(v^*) = \lim_{j \to \infty} \hat{S} \circ \hat{h}(v^k) = \lim_{j \to \infty} v^{k_j+1}$$

Then since $\hat{S} \circ \hat{h}(v^*)$ is also a limit point of v^k it must have the same distance to $\hat{v}$ as v^*

$$\|v^* - \hat{v}\| = \|\hat{S} \circ \hat{h}(v^*) - \hat{v}\| = \|\hat{S} \circ \hat{h}(v^*) - \hat{S} \circ \hat{h}(\hat{v})$$

Now using again lemma 2.2.1 we have $v^* = \hat{S} \circ \hat{h}(v^*)$.

Since $\hat{v}$ is any fixed point of $\hat{S} \circ \hat{h}$, by repalcing $\hat{v}$ with v^* in (2.14) we establish the convergence of v^k, $\lim_{k \to \infty} v^k = v^*$.

The convergence of f^k to some u^* follows from (2.11).

□

Next we develop a finite convergence property for the auxiliary variable w. Let

$$h_i(w) = (h_i^{(1)}(w), h_i^{(2)}(w), h_i^{(3)}(w)) \in \mathbb{R}^3),\ i = 1, 2, \ldots, n^2 m$$

and let L_1, L_2, E_1 and E_2 be the following index sets:

$$L_1 = \left\{ i : \|D_i f^*\| = \|h_i(v^*)\| \leq \tfrac{1}{\beta} \right\},\ L_2 = \left\{ i : |(Kf^* - g)_i| = |h_i^{(3)}(v^*)\| \leq \tfrac{\mu}{\beta} \right\}$$

$$E_1 = \{1, 2, \ldots n^2 m\} \setminus L_1 \text{ and } E_2 = \{1, 2, \ldots n^2 m\} \setminus L_2$$

Theorem 2.2.2 (finite convergence)**.** *Under Assumption 1 the sequence* $\{(w^k, z^k, f^k)\}$ *generated by Algorithm 2 from any starting point* (w^0, z^0, f^0) *satisfies* $\mathbf{w}_i^k = \mathbf{w}_i^* = 0$*, for all* $i \in L_1$*, and* $z_i^k = z_i^* = 0$*, for all* $i \in L_2$*, for all but a finite numbers of iterations that does not exceed* $\|v^0 - v^*\|^2/\omega_1^2$ *and* $\|v^0 - v^*\|^2/\omega_2^2$*, where*

$$\omega_1 = min_{i \in L_1} \left\{ \tfrac{1}{\beta} - \|h_i(v^*)\| \right\} > 0 \text{ and } \omega_2 = min_{i \in L_2} \left\{ \tfrac{\mu}{\beta} - |h_i^{(3)}(v^*)| \right\} > 0$$

We next show the q-linear convergence of f^k and the remaining components of v^k. For convenience let

$$L = L_1 \cup (n^2m + L_1) \text{ and } E = \{1, \dots n^2m\} \setminus L$$

Denote v_L the subvector of v with components (v_i), $i \in L$ and v_E be defined similarly.
Furthermore let $P = HM^{-1}H^T$ and $P_{EE} = [P_{i,j}]_{i,j \in E}$

Theorem 2.2.3 (q-linear convergence)**.** *Under Assumption 1, the sequence* $\{(w^k, z^k, f^k)\}$ *generated by Algorithm 2 satisfies:*

$$\|v_E^{k+1} - v_E^*\| \leq \sqrt{\rho(P_{EE})}\|v_E^k - v_E^*\|$$
$$\|f^{k+1} - f^*\|_M \leq \sqrt{\rho(P_{EE})}\|w_E^k - w_E^*\|_M$$

for all k sufficiently large.

2.3 Numerical results

In this section we present numerical results of recovering images by the proposed alternating minimization algorithm.

2.3.1 Test problem

In our experiments, the test problem we used to simulate breast is called CIRS: it is a three-dimensional grayscale phantom of size 128x128x15 that contains three different type of structures that simulate respectively fibers, microcalcifications and masses.

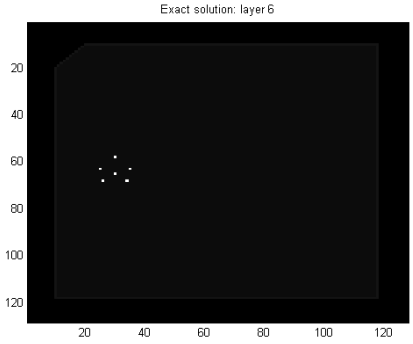

(a) layer 6

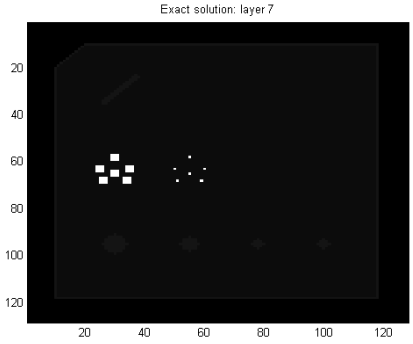

(b) layer 7

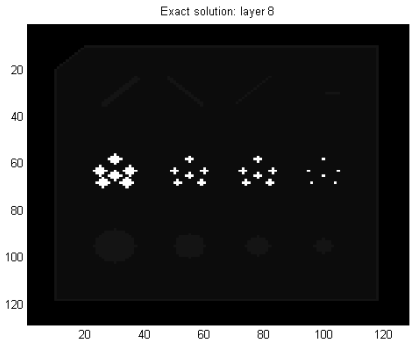

(c) layer 8 (central layer)

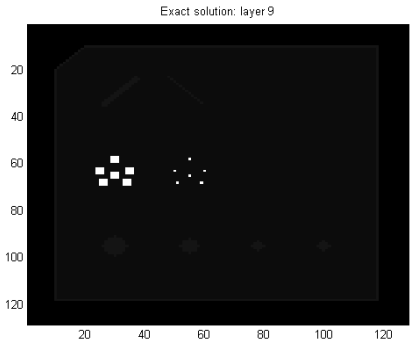

(d) layer 9

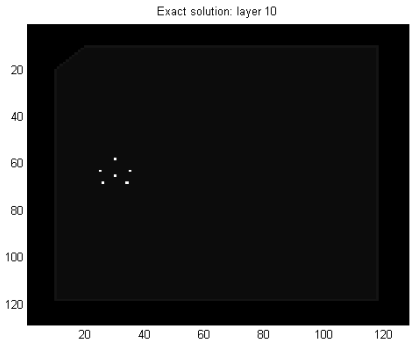

(e) layer 10

Figure 2.1: Cirs phantom

In figure 2.1 it is represented the central slice of the phantom, in which we can recognize the objects descripted above, the fibers in the first row, the

microcalcifications in the central portion and the masses in the third row, and we show also 6th, 7th, 9th and 10th layer of the model to recognize the different thicknesses of the structures in it.

As regards the construction of the matrix K, it has been obtained by using the fast algorithm for the calculus of an exact radiological path for a three-dimensional CT system presented by Robert L. Siddon in [5]. More precisely, in this work the matrix K has been constructed by using the Siddons algorithm with N = 13 equispaced projection angles from -17 to 17.

2.3.2 Numerical experiments

We set the parameters of the ADM algorithm as follows: $\mu = 50$, $\beta_1 = 0.3$, $\beta_2 = 0.1$, tollerance of the CG algorithm at 10^{-3}, and we establish a maximum number of iteration for CG equal to 50 for the first run, and equal to the number of iterations occured in the previous run by the second iteration onward.

We want to reconstruct the images starting by noisy projections with a level of noise equal to 10^{-3}.

We arrived at a relative error

$$e_{rel} = \frac{\|x^k - x_{exact}\|}{\|x_{exact}\|}$$

in the solution equal to $e_{rel} = 0.0895$, and the algorithm stopped for the condition on the maximum number of iteration in extern cycle reaching the 2000 iteration in 2600 seconds.

In Figure 2.2 we show the reconstruction obtained with the ADM algorithm, and in particular the layers from 6 to 10.

In Figure 2.3 we show the plot of the relative error at each iteration.

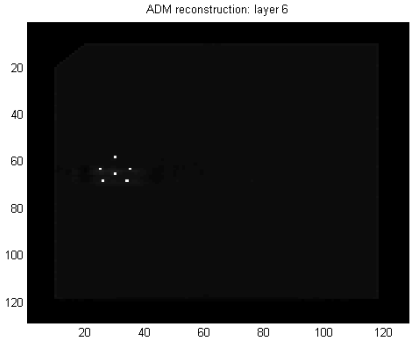

(a) Layer 6

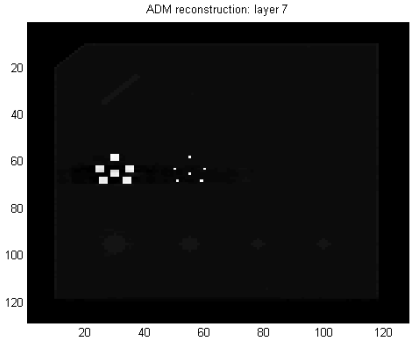

(b) Layer 7

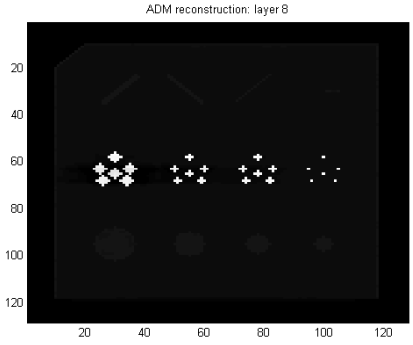

(c) Layer 8

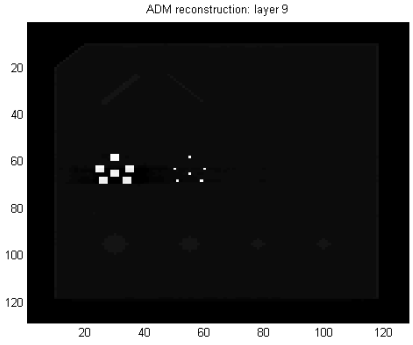

(d) Layer 9

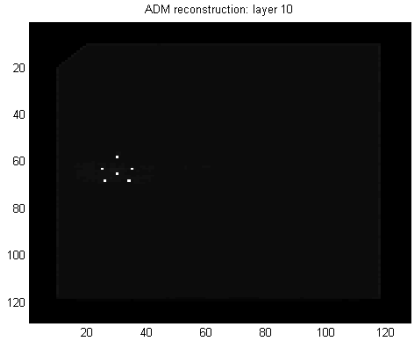

(e) Layer 10

Figure 2.2: ADM reconstruction

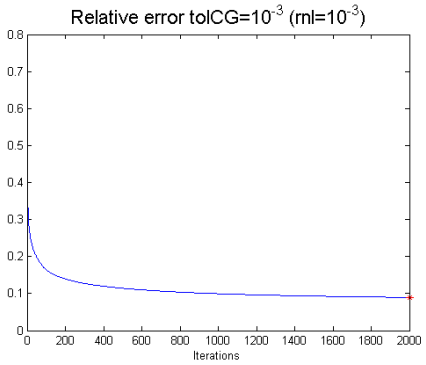

(a) relative error

Figure 2.3: ADM relative error

In Figure 2.4 and 2.5 are represent the central and the 9th layer of the ADM reconstruction and of the exact solution.

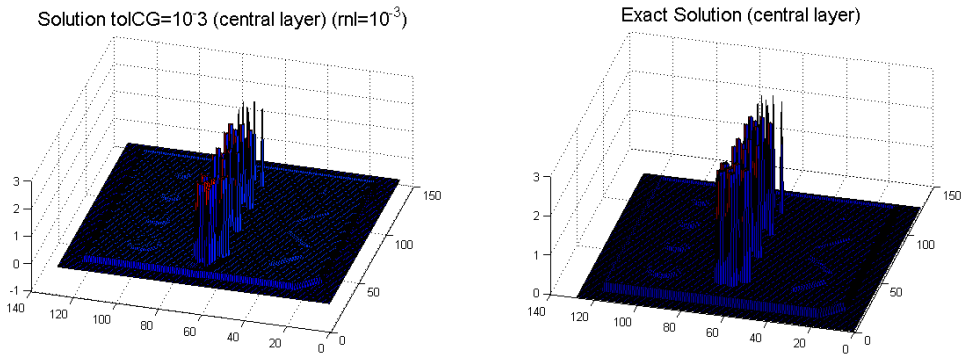

(a) ADM with tolCG=10^{-3} (b) exact images

Figure 2.4: Recostruction comparison (central layer)

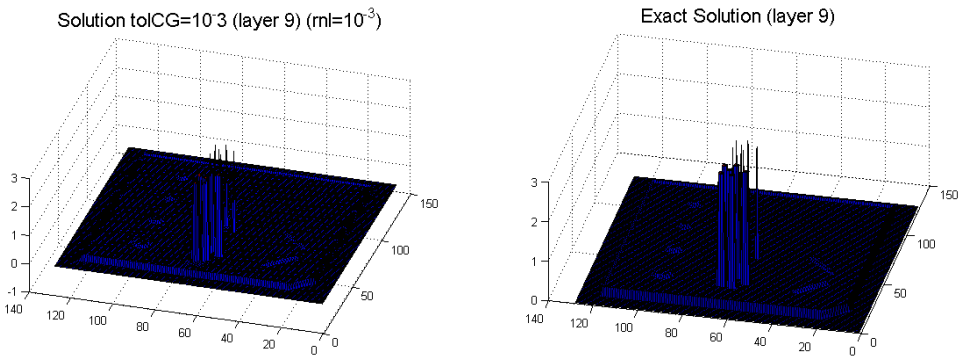

(a) ADM with tolCG=10^{-3} (b) exact images

Figure 2.5: Recostruction comparison (layer 9)

In the figures below we compare the heights of the jumps in the reconstructions with the ADM methods in relation to the jumps present in exact solution: we took into consideration the central and the ninth layer of the phantom and in particular the thirtieth, the sixty-third, and the ninety-sixth rows of both layers.

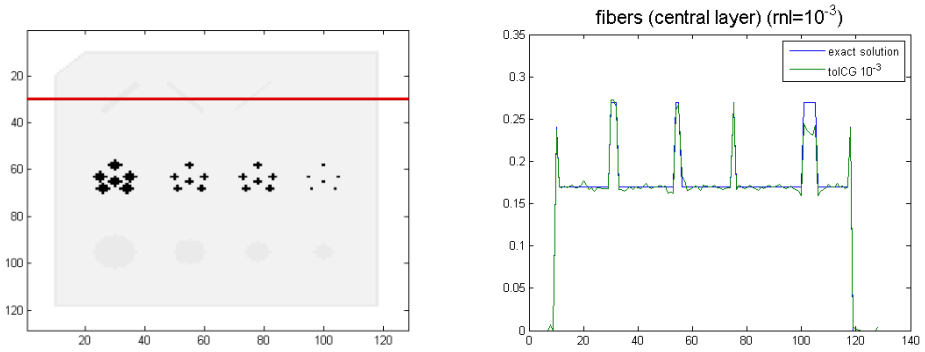

(a) fibers line (b) fibers

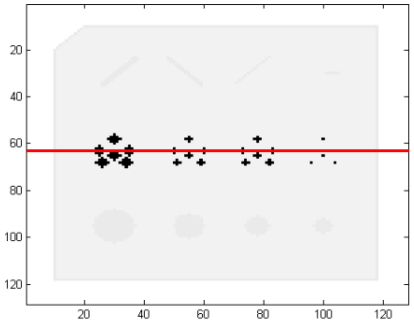

(c) microcalcification line

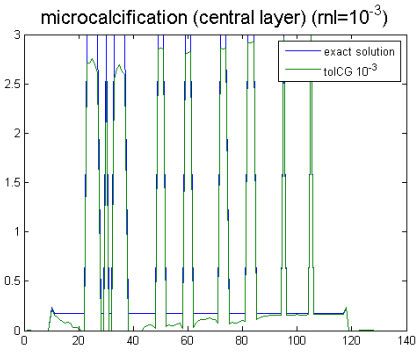

(d) microcalcification

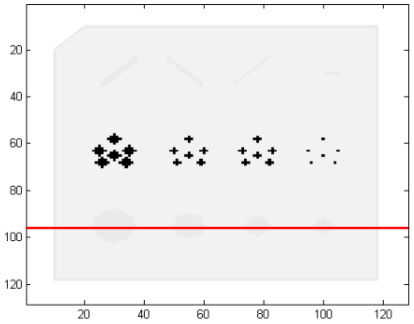

(e) masses line

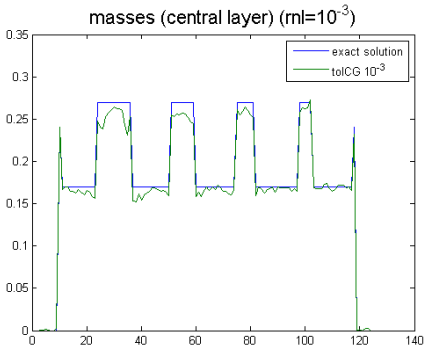

(f) masses

Figure 2.6: Comparison of the different structures recostructions (central layer)

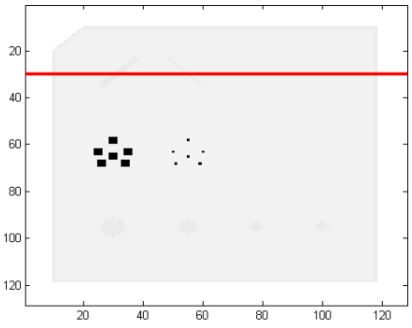

(a) fibers line

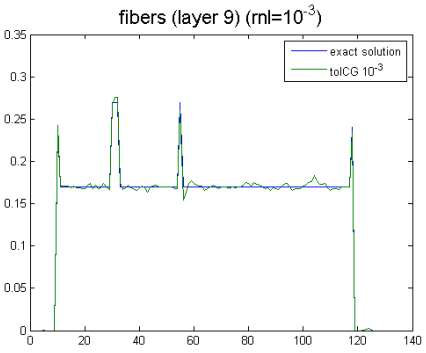

(b) fibers

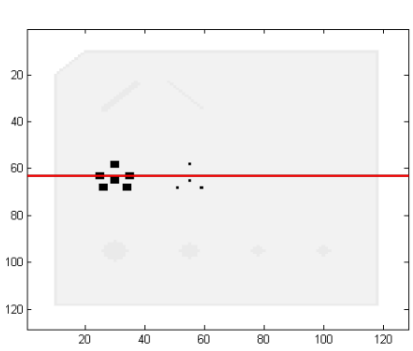

(c) microcalcification line

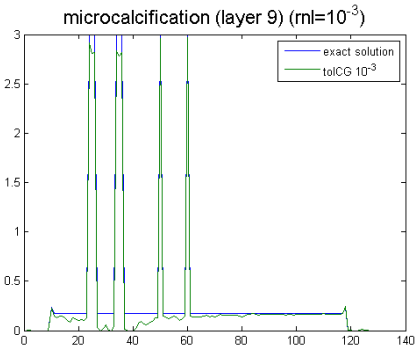

(d) microcalcification

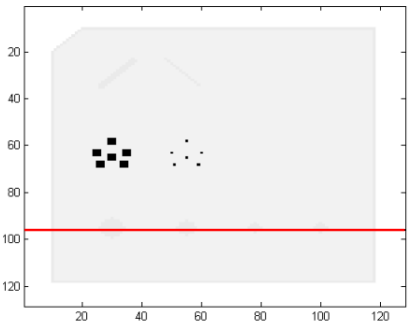

(e) masses line

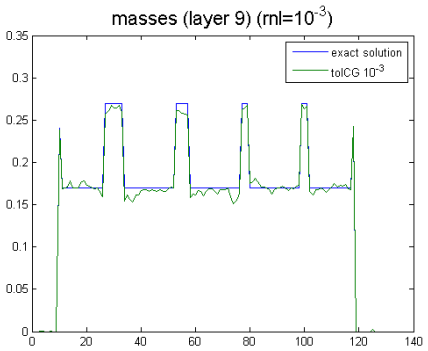

(f) masses

Figure 2.7: Comparison of the different structures recostructions (layer 9)

We now study the reconstruction stopping the iterative algorithm at 10, 30 and 60 seconds, to analyse the gradual appearence of the significant structures and the increasing quality of their reconstruction during successive iterations.

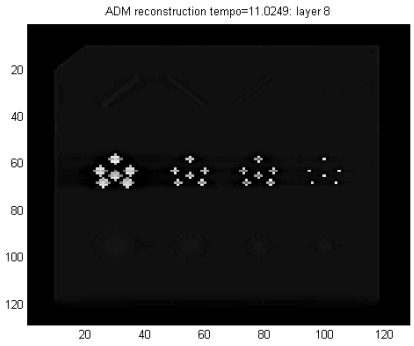

(a) 10 secs

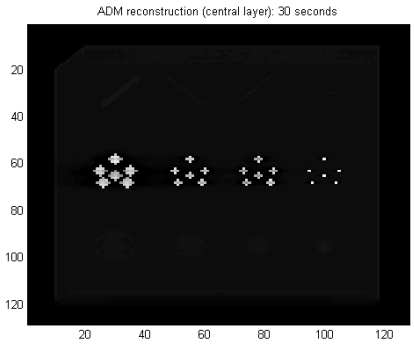

(b) 30 secs

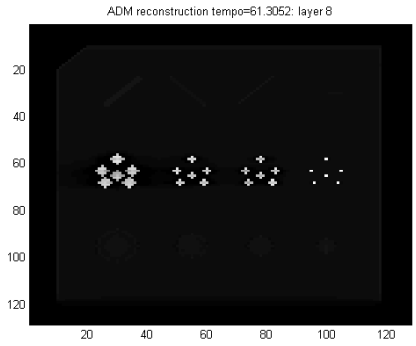

(c) 60 secs

Figure 2.8: Recostructions after 10, 30 and 60 seconds (layer 8)

In particular we show the profiles of the reconstruction inner structures stopping the iterative ADM algorithm after 30 seconds.

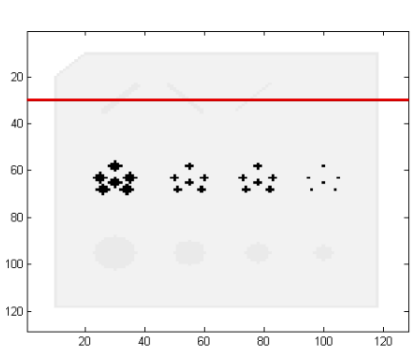

(a) fibers line

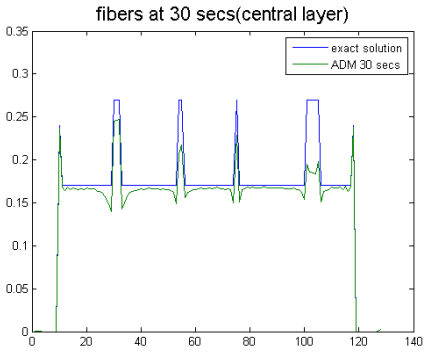

(b) fibers

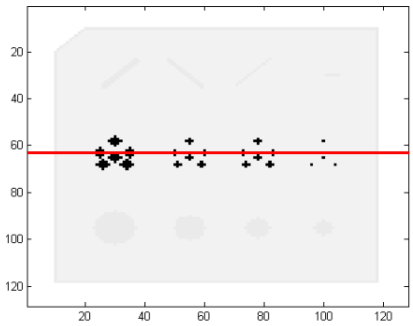

(c) microcalcification line

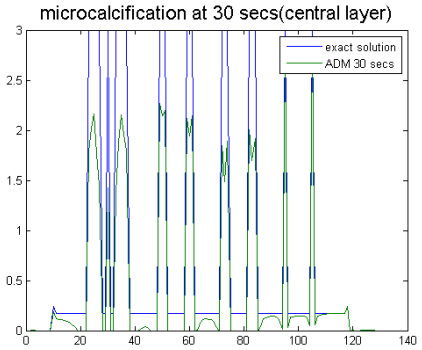

(d) microcalcification

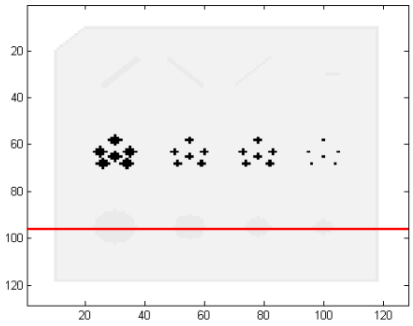

(e) masses line

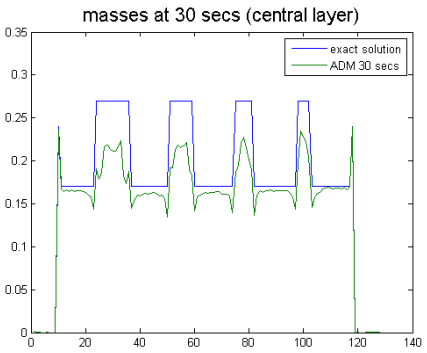

(f) masses

Figure 2.9: Comparison of the different structures recostructions after 30 seconds (central layer)

At the end we analyse the reconstruction solution with regard to the presence of noise: in particular we use as a parameter the signal-to-noise ratio (SNR).

SNR is a measure that compares the level of a desired signal to the level of background noise and is defined as the ratio of signal power to the noise power: we use the definition

$$SNR = 20\dot{\log}_{10}\left(\frac{A_{signal}}{A_{noise}}\right) \tag{2.15}$$

where A is root mean square amplitude.

Since in the test problem we consider the noise is added to the projection, and not to the exact image, we calculate A_{noise} using the difference between the exact solution and the reconstructured image we computed.

We also calculate the SNR in a region of interest (ROI), indicated in red in Figure 2.10 *(b)*, which not interesect any of the structures mentioned above to better measure noise level in the background.

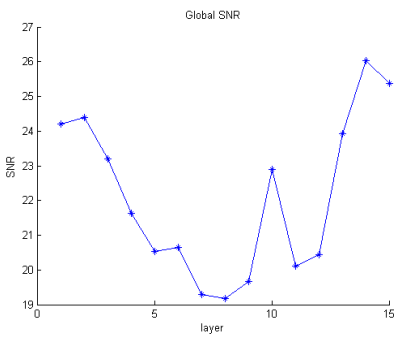

(a) Global SNR

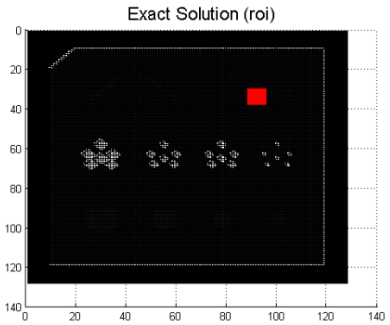

(b) ROI

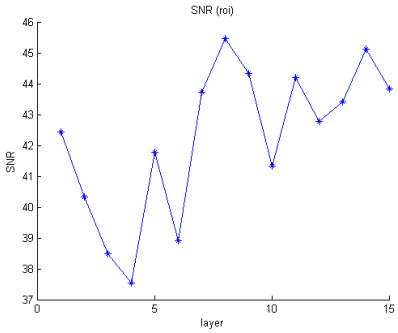

(c) SNR in the ROI

Figure 2.10: SNR in each layer

Chapter 3

Scaled Projected Gradient Method

In this chapter we introduce a scaled gradient projection (SGP) method for solving the problem introduced in the Chapter 1, interpretated like a constrained minimization problem of the general form

$$\min f(x) \quad \text{s. t. } x \in \Omega \tag{3.1}$$

3.1 Definition and basic properties

Given the optimization problem (3.1), we recall that $x^* \in \Omega$ is a stationary point of f over Ω if

$$-\nabla f(x^*)^T(y - x^*) \leq 0, \quad \forall y \in \Omega$$

or, if Ω is convex, if $-\nabla f(x^*)^T w \leq 0$ for any w in the tangent cone of Ω at x^*.

Let $\Omega \subset \mathbb{R}^N$ be a closet convex set and D be a symmetric positive definite

$N \times N$ matrix, we define the projection operator $P_{\Omega,D} : \mathbb{R}^N \to \Omega$ as

$$P_{\Omega,D} \equiv \arg\min_{y\in\Omega} ||y - x||_D = \arg\min_{y\in\Omega} \left(\phi(y) \equiv \frac{1}{2} y^T D y - y^T D x \right) \tag{3.2}$$

We observe that the operator $P_{\Omega,D}$ is a continuous function with respect to the elements of the matrix D and that is defined also by

$$(P_{\Omega,D}(x) - x)^T D (P_{\Omega,D}(x) - y) \leq 0 \quad \forall y \in \Omega \tag{3.3}$$

Let $\mathcal{D}_L \in \mathbb{R}^{N\times N}$ be the compact set of the symmetric positive definite $N \times N$ matrices such that $||D|| < L$ and $||D^{-1}|| < L$, for a given threshold $L > 1$. The following lemmas state two basic properties related to the projection operator: a Lipschitz continuity condition and a characterization for the stationary points of problem (3.1); we omit the proofs but the reader can find them in [6].

Lemma 3.1.1. *If $D \in \mathcal{D}_L$, then*

$$||P_{\Omega,D}(x) - P_{\Omega,D}(z)|| \leq L^2 ||x - z||$$

for any $x, z \in \mathbb{R}^N$

Lemma 3.1.2. *A vector $x_* \in \Omega$ is a stationary point of the problem (3.1) if and only if $x_* = P_{\Omega,D^{-1}}(x_* - \alpha D \nabla f(x_*))$ for any positive scalar α and for any symmetric positive definite matrix D.*

3.2 The SGP method

The second lemma shows the effect of the projection operator $P_{\Omega,D^{-1}}$ on the points $x_* - \alpha D \nabla f(x_*), \alpha > 0$, when x_* is a stationary point of (3.1). In the case $\bar{x} \in \Omega$ is a nonstationary point, $P_{\Omega,D^{-1}}(\bar{x} - \alpha D \nabla f(\bar{x}))$ can be exploited

to generate a descend direction for the function f in $\bar{x}$. This idea serves as the basis for the SGP method.

Algorithm 3: SGP (scaled gradient projecion) method

Given $x_0 \in \Omega$, $\beta, \gamma \in (0,1)$, $0 < \alpha_{min} < \alpha_{max}$, *and fix a positive integer* M.

for $k = 0, 1, 2, \cdots$ **do**

STEP 1. Choose the parameter $\alpha_k \in [\alpha_{min}, \alpha_{max}]$ *and the scaling matrix* $D_k \in \mathcal{D}_L$;

Projection: $y^{(k)} = P_{\Omega, D_k^{-1}}(x^{(k)} - \alpha_k D_k \nabla f(x^{(k)}))$;

if $y^{(k)} = x^{(k)}$ **then**

STEP 2. Stop declaring that $x^{(k)}$ *is a stationary point*

end

STEP 3. Descend direction: $d_{(k)} = y^{(k)} - x^{(k)}$;

STEP 4. Set $\lambda_k = 1$ *and* $f_{max} = \max_{0 \le j \le min(k, M-1)} f(x^{(k-j)})$;

STEP 5. Backtracking loop:

if $f(x^{(k)} + \lambda_k d^{(k)}) \le f_{max} + \beta \lambda_k \nabla f(x^{(k)})^T d^{(k)}$ **then**

go to STEP 6;

else

set $\lambda_k = \theta_k$ *and go to the STEP 5.*;

end

STEP 6. Set $x^{(k+1)} = x^{(k)} + \lambda_k d^{(k)}$.

end

If the projection performed in STEP 2 returns a vector $y^{(k)} = x^{(k)}$, then lemma (3.1.2) implies that $x^{(k)}$ is a stationary point and the algorithm stops. When $y^{(k)} \neq x^{(k)}$, it is possible to prove that $d^{(k)}$ is a descent direction for f in $x^{(k)}$ and the backtracking loop in STEP 5 terminates with finite number of runs.

The nonmonotone line-search strategy implemented in STEP 5 ensures that

$f(x^{(k+1)})$ is lower than the maximum of the objective function on the last M iterations; if $M = 1$ then the strategy reduces to the standard monotone Armijo rule.

3.3 Convergence analysis

The main SGP convergence result is stated in theorem 2.2.1, whose proof is based on some crucial properties that we report in the following lemmas: the first two lemmas are concerned with the descend condition and the boundedness of the direction $d^{(k)}$, respectively.
We will focus on the case in which the algorithm generates an infinite sequence of iterates, denoted by $\{x^{(k)}\}$.

Lemma 3.3.1. *Assume that $d^{(k)} \neq 0$. Then $d^{(k)}$ is a descend direction for the functional f at $x^{(k)}$, that is, $\nabla f(x^{(k)})^T d^{(k)} < 0$.*

Lemma 3.3.2. *If the sequence $\{x^{(k)}\}$ generated by the SGP algorithm is bounded, then also the sequences $d^{(k)}$ is bounded.*

Now we state two properties of the accumulation points of the sequence generated by SGP.

Lemma 3.3.3. *Assume that the subsequence $\{x^{(k)}\}_{k\in K}$, $K \subset \mathbb{N}$, is converging to a point $x_* \in \Omega$. Then, x_* is a stationary point of (3.1) if and only if*

$$\lim_{k\in K} \nabla f(x^{(k)})^T d^{(k)} = 0$$

Lemma 3.3.4. *Let $x_* \in \Omega$ be an accumulation point of the sequence $\{x^{(k)}\}$ such that $\lim_{k\in K} x^{(k)} = x_*$, for some $K \subset \mathbb{N}$. If x_* is a stationary point of*

(3.1), then x_* is an accumulation point also for the sequence $\{x^{(k+r)}\}_{k\in K}$ for any $r \in \mathbb{N}$. Furthermore,

$$\lim_{k\in K} ||d^{(k+r)}|| = 0 \quad \forall r \in \mathbb{N}$$

At this point we may state a convergence result for SGP:

Theorem 3.3.1. *Assume that the level set $\Omega_0 = \{x \in \Omega : f(x) \leq f(x^{(0)})\}$ is bounded. Every accumulation point of the sequence $\{x^{(k)}\}$ generated by the SGP algorithm is a stationary point of (3.1).*

Proof. Since every iterate $x^{(k)}$ lies in Ω_0, the sequence $\{x^{(k)}\}$ is bounded and has at least one accumulation point. Let $x^* \in \Omega$ be such that $\lim_{k\in K} x^{(k)}$ for a set of indices $K \subset \mathbb{N}$.
We consider two cases:

a) $\inf_{k\in K} \lambda_k = 0$;

b) $\inf_{k\in K} \lambda_k = \rho > 0$.

Case a. Let $K_1 \subset K$ be a set of indices such that $\lim_{k\in K_1} \lambda_k = 0$. That implies that, for $k \in K_1$, k sufficiently large, the backtracking rule fails to be satisfied at least once. Thus, at the penultimate step of the backtracking loop, we have

$$f\left(x^{(k)} + \frac{\lambda_k}{\theta} d^{(k)}\right) > f(x^{(k)} + \beta \frac{\lambda_k}{\theta} \nabla f(x^{(k)})^T d^{(k)}$$

hence

$$\frac{f(x^{(k)} + \frac{\lambda_k}{\theta} d^{(k)}) - f(x^{(k)}}{\frac{\lambda_k}{\theta}} > \beta \nabla f(x^{(k)})^T d^{(k)} \tag{3.4}$$

By the mean value theorem, we have that there exists a scalar $t_k \in [0, \frac{\lambda_k}{\theta}]$ such that the left-hand side of (3.4) is equal to $\nabla f(x^{(k)} + t_k d^{(k)})^T d^{(k)}$. Thus the inequality (3.4) becomes

$$\nabla f(x^{(k)} + t_k d^{(k)})^T d^{(k)} > \beta \nabla f(x^{(k)})^T d^{(k)} \tag{3.5}$$

Since α_k and D_k are bounded, it is possible to find a set of indices $K_2 \in K$ such that $\lim_{k \in K_2} \alpha_k = \alpha_*$ and $\lim_{k \in K_2} D_k = D_*$. Thus the sequence $d^{(k)}{}_{k \in K_2}$ converges to a vector $d_* = (P_{\Omega, D_*^{-1}}(x_* - \alpha_* D_* \nabla f(x_*)) - x_*)$ and, furthermore, $t_k d^{(k)} \to 0$ when k diverges, $k \in K_2$. Taking limits in (3.5) as $k \to \infty$, $k \in K_2$, we obtain

$$(1 - \beta) \nabla f(x_*)^T d_* < 0$$

Since $(1 - \beta) > 0$ and $\nabla f(x_*)^T d_* < 0$ for all k, then we necessarily have $\lim_{k \in K_2} \nabla f(x^{(k)})^T d^{(k)} = \nabla f(x_*)^T d_* = 0$. Then by lemma 3.3.3, we conclude that x_* is a stationary point.

Case b. Let us define the point $x^{(l(k))}$ as the point such that

$$f(x^{(l(k))}) = f_{max} = max_{0 \leq j \leq min(k, M-1)} f(x^{(k-j)})$$

Then, for $k > M - 1$, $k \in \mathbb{N}$, the following condition holds:

$$f(x^{(l(k))}) \leq f(x^{(l(l(k)-1)))}) + \beta \lambda_{l(k)-1} \nabla f(x^{(l(k)-1)})^T d^{(l(k)-1)} \tag{3.6}$$

Since the iterates $x^{(k)}$, $k \in \mathbb{N}$ belong to a bounded set, the monotone non-increasing sequence $\{f(x^{(l(k))})\}$ admits a finite limit $\mathcal{L} \in \mathbb{R}$ for $k \in K$. Let $K_3 \subset K$ be a set of indices such that $\lim_{k in K_3} \lambda_{l(k)-1} = \rho_1 \geq \rho > 0$ and $\lim_{k \in K_3} \nabla f(x^{(l(k)-1)})^T d^{(l(k)-1)}$ exists; taking limits on (3.6) for $k \in K_3$ we obtain

$$\mathcal{L} \leq \mathcal{L} + \beta \rho_1 \lim_{k \in K_3} \nabla f(x^{(l(k)-1)})^T d^{(l(k)-1)}$$

that is

$$\lim_{k \in K_3} \nabla f(x^{(l(k)-1)})^T d^{(l(k)-1)} \geq 0$$

Recalling that $\nabla f(x^{(k)})^T d^{(k)} < 0$ for any k, the previous inequality implies that

$$\lim_{k \in K_3} \nabla f(x^{(l(k)-1)})^T d^{(l(k)-1)} = 0 \tag{3.7}$$

Then by lemma 3.3.3, (3.7) implies that every accumulation point of the sequence $\{x^{(l(k)-1)}\}_{k \in K_3}$ is a stationary point of (3.10).

Let us prove that the point x_* is an accumulation point of $\{x^{(l(k)-1)}\}_{k \in K_3}$.

The definition of $x^{(l(k))}$ implies that $k - M + 1 \leq l(k) \leq k$. Thus we can write

$$\|x^{(k)} - x^{(l(k)-1)}\| \leq \sum_{j=0}^{k-l(k)} \lambda_{l(k)-1+j} \|d^{(l(k)-1+j)}\|, \quad k \in K \tag{3.8}$$

Let $K_4 \subset K$ be a subset of indices such that the sequence $\{x^{l(k)-1)}\}_{k \in K_4}$ converges to an accumulation point $\bar{x} \in \Omega$. Recalling that, from (3.7) and lemma 3.3.3, $\bar{x}$ is a stationary point of (3.10), we can apply lemma 3.3.4 to obtain that $\lim_{k \in K_4} \|d^{(l(k)-1+j)}\| = 0$ for any $j \in \mathbb{N}$. By using (3.8) we conclude that

$$\lim_{k \in K_4} \|x^{(k)} - x^{(l(k)-1)}\| = 0 \tag{3.9}$$

Since $\|x_* - x^{(l(k)-1)}\| \leq \|x^{(k)} - x^{(l(k)-1)}\| + \|x^{(k)} - x_*\|$ and $\lim_{k \in K} x^{(k)} = x_*$, then (3.9) implies that x_* is an accumulation point also for the sequence $\{x^{(l(k)-1)}\}_{k \in K_3}$. Hence, we conclude that x_* is a stationary point of (3.10). □

3.4 The SGP method for 3D image reconstruction

In this section we describe SGP implementation for solving special costrained minimization problems arising in 3D image reconstruction. We consider the constrained minimization problem of the form

$$\min T(f) \quad \text{s. t. } f \geq 0 \tag{3.10}$$

where T is a continuous differentiable convex function measuring the difference between reconstructured and measures data, and containing a penalty term expressing additional information on the solution, while the constraint force the nonnegativity of the solution.
In this work

$$T(f) = ||Kf - b||_1 + \lambda * TV(f) \tag{3.11}$$

where $TV(f)$ is a discrete approximation of the Total Variation.

3.4.1 Update the scaling matrix

The choice of the scaling matrix D_k in SGP must aim at two main goals: avoiding to introduce significant computational costs and improving the convergence rate.
A classical choice is to use a diagonal scaling matrix $D_k = diag(d_1^{(k)}, d_2^{(k)}, \cdots, d_N^{(k)})$ and in this thesis we will use the following updating rule

$$d_i^{(k)} = min\left\{L, max\left\{\frac{1}{L}, x_i^{(k)}\right\}\right\}, i = 1, \cdots, N$$

In the experiments of Section 3.5 we take $L = 10$.

3.4.2 Update the steplength

Steplenght selection rules in gradient methods have received an increasing interest in the last years from both the theoretical and the practical point of view in order to accelerate the slow convergence exibithed in most cases by standard gradient method.
To this end, we can regard the matrix $B(\alpha_k) = (\alpha_k D_k)^{-1}$ as an approximation of the Hessian $\nabla^2 J(x^{(k)})$, and derive two updating rules for α_k using the secant equation.

We use the approximation $\nabla^2 J(x^{(k)})(x_k - x_{k-1}) \approx \nabla J(x_k) - \nabla J(x_{k-1})$ and derive the equation

$$B(\alpha_k)(x_k - x_{k-1}) = \nabla J(x_k) - \nabla J(x_{k-1}) \tag{3.12}$$

From (3.12) we obtain two different equation for α_k (SC1) and (SC2), which will bring us two different updating rules. We have

$$\alpha_k^{SC1} = \arg\min_{\alpha_k \in \mathbb{R}} ||B(\alpha_k)s^{(k-1)} - z^{(k-1)}||$$

and

$$\alpha_k^{SC2} = \arg\min_{\alpha_k \in \mathbb{R}} ||s^{(k-1)} - B(\alpha_k)^{-1} z^{(k-1)}||$$

where $s^{(k-1)} = (x^{(k)} - x^{(k-1)})$ and $z^{(k-1)} = (\nabla J(x^{(k)}) - \nabla J(x^{(k-1)}))$.
In this way we have

$$\alpha_k^{(1)} = \frac{s^{(k-1)^T} D_k^{-1} D_k^{-1} s^{(k-1)}}{s^{(k-1)} D_k^{-1} z^{(k-1)}} \tag{3.13}$$

and

$$\alpha_k^{(2)} = \frac{s^{(k-1)^T} D_k z^{(k-1)}}{z^{(k-1)} D_k D_k z^{(k-1)}} \tag{3.14}$$

and we use a steplength updating rule for SGP which adaptively alternates the values provided by (3.13) and (3.14).

Algorithm 4: SGP steplength selection

if $k=0$ **then**

  set $\alpha_0 \in [\alpha_{min}, \alpha_{max}], \tau_1 \in (0,1)$ *and a non-negative integer* M_α ;

else

  if $s^{(k-1)} D_k^{-1} z^{(k-1)} \leq 0$ **then**

    $\alpha_k^{(1)} = \alpha_{max}$;

  else

    $\alpha_k^{(1)} = \max\left\{\alpha_{min}, \min\left\{\frac{s^{(k-1)^T} D_k^{-1} D_k^{-1} s^{(k-1)}}{s^{(k-1)} D_k^{-1} z^{(k-1)}}, \alpha_{max}\right\}\right\}$;

  end

  if $s^{(k-1)^T} D_k z^{(k-1)} \leq 0$ **then**

    $\alpha_k^{(2)} = \alpha_{max}$

  else

    $\alpha_k^{(2)} = \max\left\{\alpha_{min}, \min\left\{\frac{s^{(k-1)^T} D_k z^{(k-1)}}{z^{(k-1)} D_k D_k z^{(k-1)}}, \alpha_{max}\right\}\right\}$;

  end

  if $\frac{\alpha_k^{(2)}}{\alpha_k^{(1)}} \leq \tau_k$ **then**

    $\alpha_k = \min\left\{\alpha_j^{(2)}, j = \max 1, k - M_\alpha, \cdots, k\right\}$;

    $\tau_{k+1} = \tau_k \cdot 0.9$;

  else

    $\alpha_k = \alpha_k^{(1)}$;

    $\tau_{k+1} = \tau_k \cdot 1.1$;

  end

end

3.5 Numerical results

The experiments on this section test the considered SGP method for 3D image restoration, and in particular our test problem is the one described in

Chapter 2.

As we said before, we will consider the problem in the form (3.10) and we will use objective function $T(x)$ defined as (3.11).

We study the SGP behaviour using the scaling matrix D_k defined as in Section 3.5, and the steplength α_k defined by the alternating $\alpha_k^{(1)}$ and $\alpha_k^{(2)}$ as in the Algorithm 4, by setting $M_\alpha = 0$, $\tau_1 = 0.15$, $[\alpha_{min}, \alpha_{max}] = [10^{-3}, 10^7]$, $\alpha_0 = 10^{-2}$.

The line-search parameter are: $\theta = 0.4$, $\beta = 10^{-4}$ and $M = 25$.

We decided to stop the algorithm if the difference $\|x^{(k+1)} - x^{(k)}\| < 10^{-8}$. In our experiment the SGP algorithm terminates at 1553 iteration.

As done with the ADM algorithm we want to reconstruct the images starting by noisy projections with a level of noise equal to 10^{-3}.

We managed to reach a relative error of $e_{rel} = 0.095$ in 2722 seconds.

The figures in Figure 3.1 below show the solution restored with the SGP algorithm from layer 6 to layer 10. Figure 3.2 shows the relative error of the reconstruction at each iteration. In particular we notice that the relative error drops to a value close to a minimum in the first iterations, and it remains close to this value for a large number of iteration; this suggested that the choice of the optimal number of iterations does not seem to be critical.

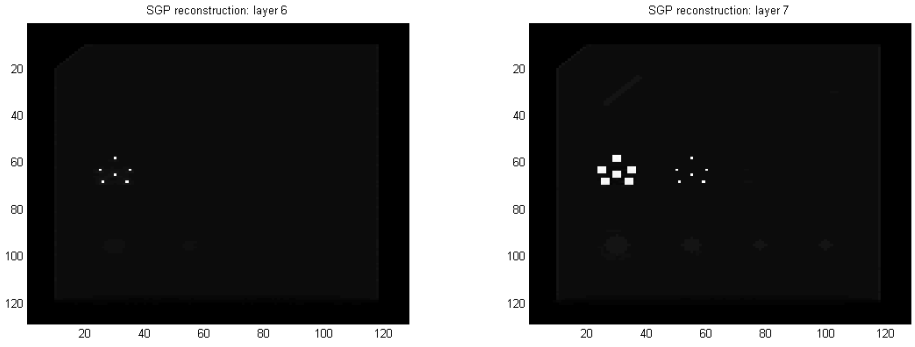

(a) Layer 6 (b) Layer 7

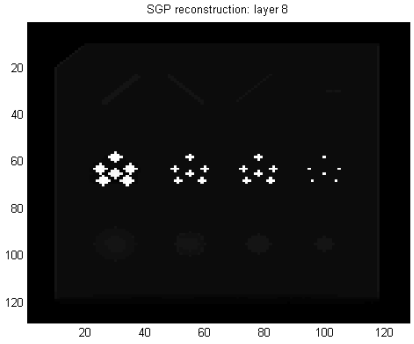

(c) Layer 8

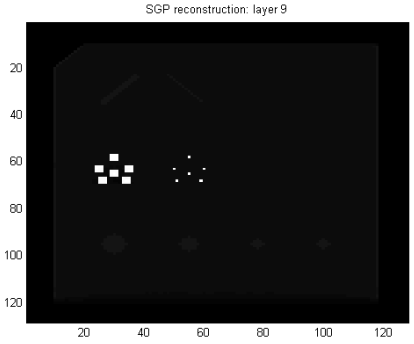

(d) Layer 9

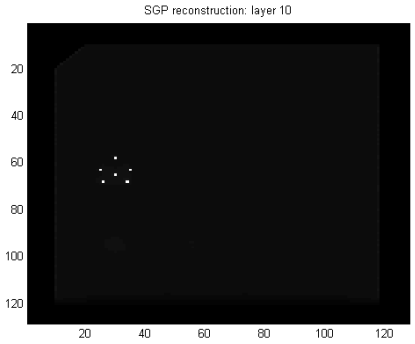

(e) Layer 10

Figure 3.1: SGP reconstruction

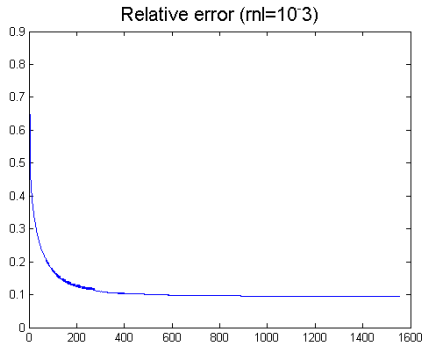

Figure 3.2: SGP relative error

The figures *(a)* and *(b)* of 3.3 give a better view of the central layer of the reconstructed image in relation to the central layer of the exact solution in order to appreciate the amplitude of the jumps obtained with the reconstruction. In figure 3.4 we did the same for the ninth layer.

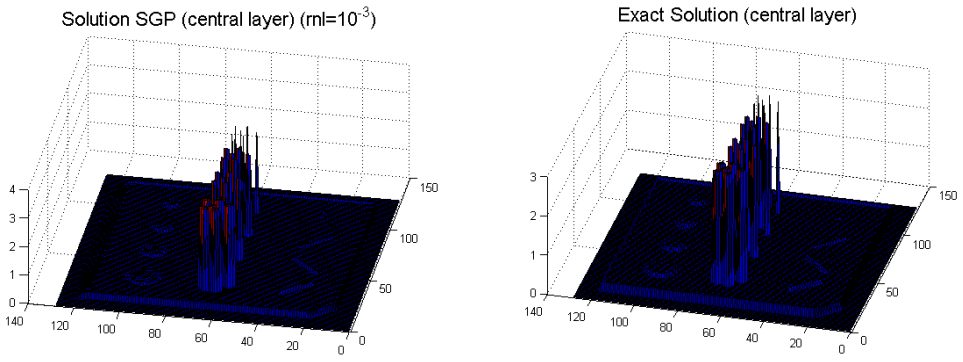

(a) SGP reconstruction (b) exact images

Figure 3.3: Recostruction comparison (central layer)

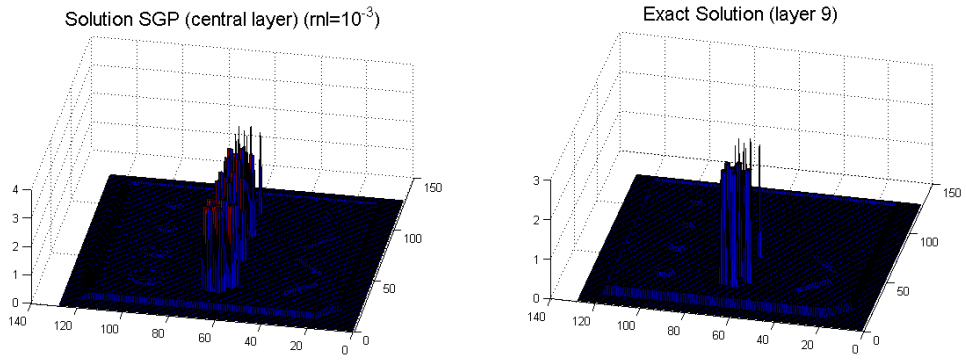

(a) SGP reconstruction (b) exact images

Figure 3.4: Recostruction comparison (layer 9)

Then we select, both in the central layer and in the ninth layer of the 3D image, the rows of pixels that run into the principal structures represented in the CIRS model, namely fibers, microcalcifications and masses, and we compare their profile with the exact solution.

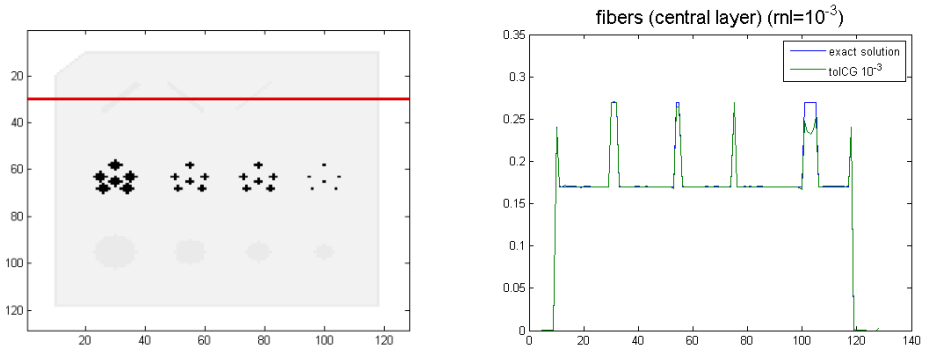

(a) fibers line (b) fibers

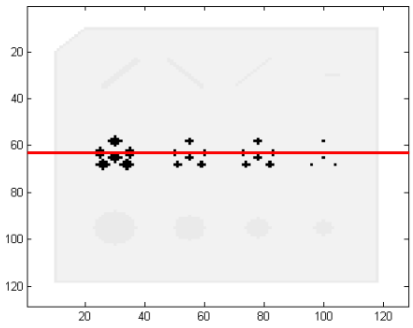

(c) microcalcification line

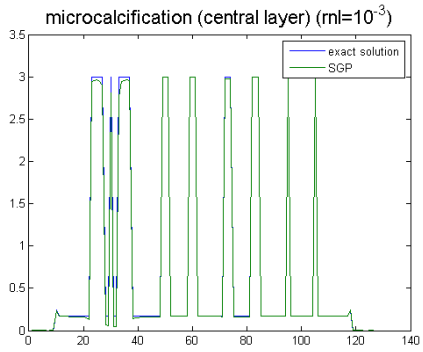

(d) microcalcification

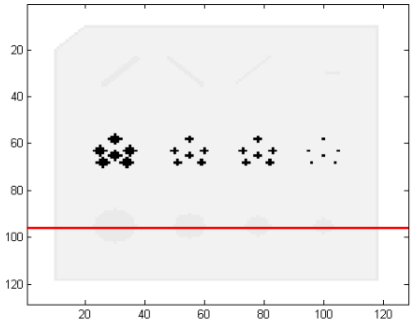

(e) masses line

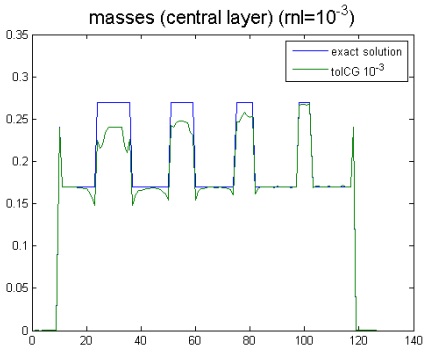

(f) masses

Figure 3.5: Comparison of the different structures recostructions (central layer)

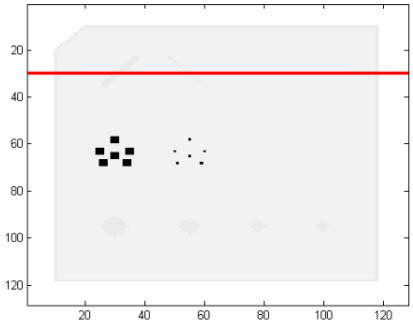

(a) fibers line

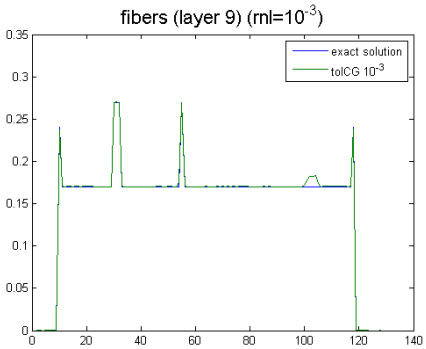

(b) fibers

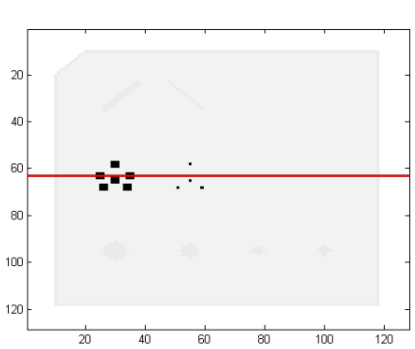

(c) microcalcification line

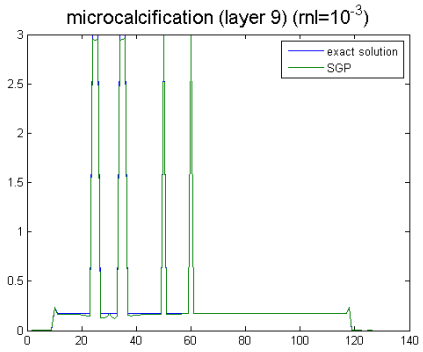

(d) microcalcification

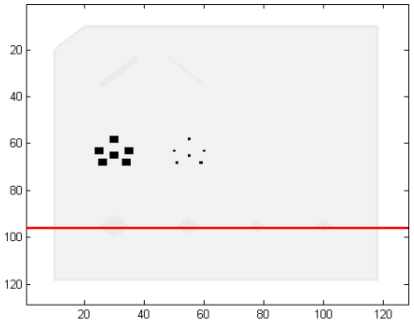

(e) masses line

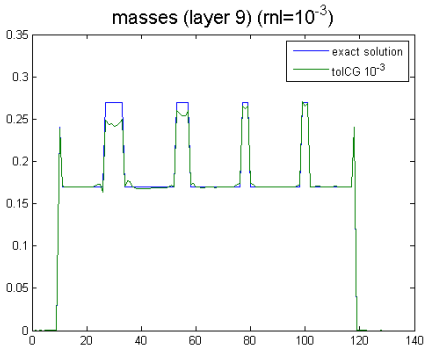

(f) masses

Figure 3.6: Comparison of the different structures recostructions (layer 9)

In Figure 3.7 we show as the structures present in the computed solution changes in time, stopping the iterative algorithm after 10, 30 and 60 seconds.

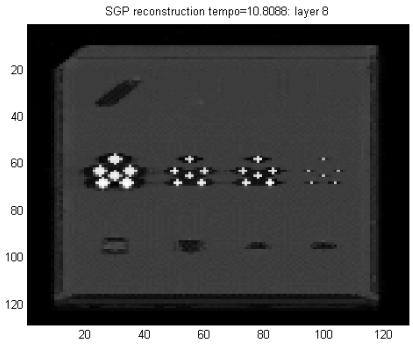

(a) 10 secs

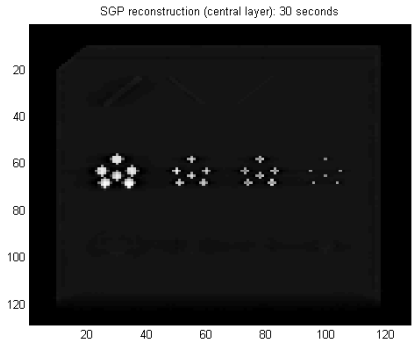

(b) 30 secs

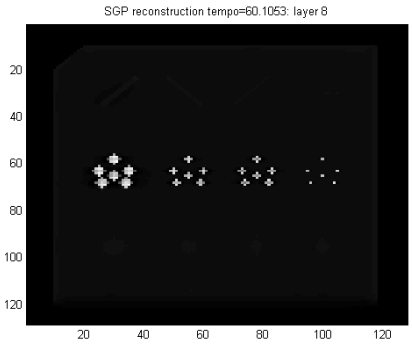

(c) 60 secs

Figure 3.7: Recostructions after 10, 30 and 60 seconds (layer 8)

In particular we show the profiles of the reconstruction inner structures stopping the iterative SGP algorithm at 30 seconds.

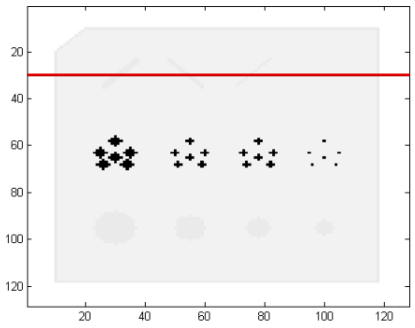

(a) fibers line

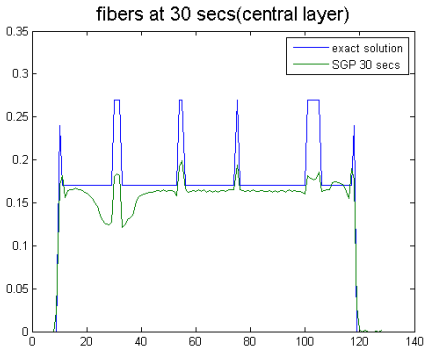

(b) fibers

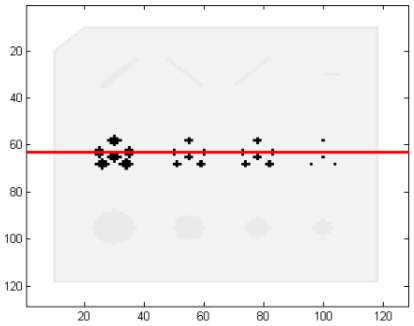

(c) microcalcification line

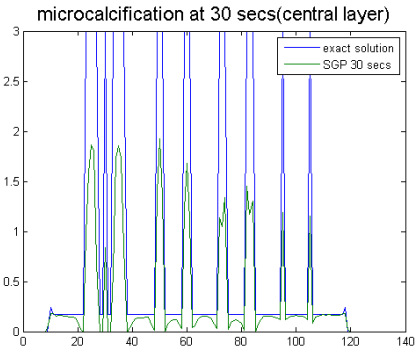

(d) microcalcification

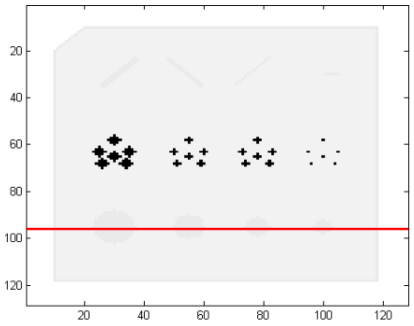

(e) masses line

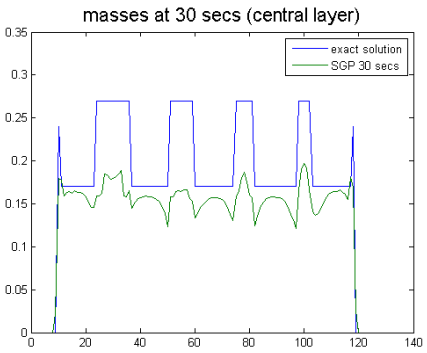

(f) masses

Figure 3.8: Comparison of the different structures recostructions after 30 seconds (central layer)

As we did for the alternating minimization algorithm of Chapter 2 we investigate the noise presence in reconstruction image by computing the SNR both in the whole 3D image and in the region of interest (ROI) indicates in red in Figure 3.9

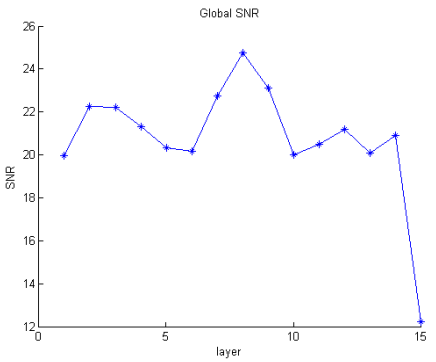

(a) Global SNR

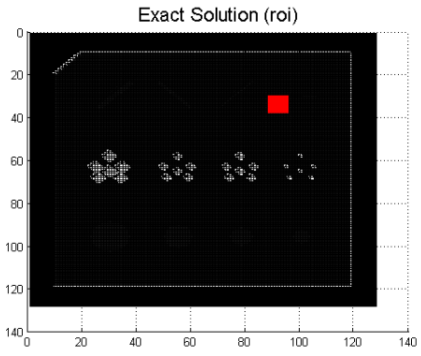

(b) ROI

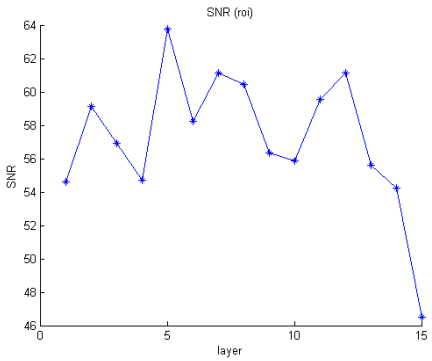

(c) SNR in the ROI

Figure 3.9: SNR in each layer

Conclusions

A DT data acquisition includes measuring a limited number of low-dose two-dimensional projections of an object, so the limited number of data leads to consider compressed sensing.

In this thesis we formulate the DT image reconstruction problem as a minimization problem involving the 1-norm and the Total Variation in order to increase the sparsity of the solution computed.

We presented in particular two different iterative algorithms: a new alternating minimization methods, and a scaled projected gradient method with the 1-norm of data fitting.

We tested the two methods with a choice of the parameters of the algorithms designed to be optimal in achieving a level of relative error that was as low as possible. Performing this choice we realized that the algorithm ADM is much less stable in the choice of parameters, namely the setting of these parameters is very sensitive and depends on the problem on which we test the algorithm, while the algorithm SGP is more stable and the choice of parameters is more versatile.

Despite this, once we set the parameters for the algorithm, ADM is faster than SGP algorithm: not only it takes less time to reach a good level of relative error in the calculation of the solution to convergence, but we noticed a more precocious and more qualitative appearance of the internal structures

of CIRS already in the reconstructions performed in the first seconds. In particular, we note the appearance of the structures that simulate the masses, which are generally structures to appear later in the iterative reconstructions, already in the first few iterations, while with the SGP algorithm they will appear with comparable quality only later.

An analysis of the final solution calculated by the two algorithms shows that both the algorithms reach the same relative error, of around 0.9, but looking at the profiles of the masses, fibers, and microcalcifications reported in the figures of Section 2.3 and 3.5 we noticed that the SGP algorithm reconstruction maintains a more uniform and less uneven profile between the jumps that represent the inner structures.

In addition, the solution calculated by the ADM has more noise than the SGP's one, with a slightly lower SNR value calculated on the ROI.

In conclusion the use of the 1-norm and the Total Variation are valid tools in the formulation of the minimization problem for the image reconstruction resulting from Digital Tomosynthesis and the new algorithm ADM has reached a relative error comparable to a version of the classic algorithm SGP and proved best in speed and in the early appearance of the structures representing the masses.

Bibliography

[1] C.R. VOGEL, *Computational Methods for Inverse Problems*. SIAM, 2002.

[2] J. NOCEDAL, S.J. WRIGHT, *Numerical Optimization*. 2nd ed. Springer (2006).

[3] Y. WANG, J. YANG, W. YIN and Y. ZHANG, *A New Alternating Minimization Algorithm for Total Variation Image Recostruction*. SIAM J. Imaging Sciences, Vol 1, No. 3, pp 248-272, 2008.

[4] Y. WANG, J. YANG, W. YIN and Y. ZHANG, *An efficient TVL1 algorithm for deblurring multichannel images corrupted by impulsive noise*. SIAM J. Sci. Comput, Vol 31, No. 4, pp 2842-2865, 2009.

[5] R. L. SIDDON, *Fast calculation of the exact radiological path for a three-dimensional CT array*. Medical Physics, 12, 252 (1985).

[6] S.BONETTINI, R. ZANELLA and L.ZANNI, *A scaled gradient projection method for constrained image deblurring*. Università di Ferrara, 2009